Available online at www.sciencedirect.com
SCIENCE DIRECT®
International Journal of Mass Spectrometry 230 (2003) 123–133
International Journal of Mass Spectrometry
www.elsevier.com/locate/ijms

A tandem mass spectrometric study of the *N*-oxides, quinoline *N*-oxide, carbadox, and olaquindox, carried out at high mass accuracy using electrospray ionization

Xiu-Sheng Miao, Raymond E. March*, Chris D. Metcalfe

Department of Chemistry, Water Quality Centre, Trent University, Peterborough, Ont., Canada K9J 7B8

Received 5 May 2003; accepted 13 August 2003

Dedicated to Professor John H. Beynon, FRS, on the occasion of his eightieth birthday

Abstract

A mass spectrometric study of three *N*-oxides, quinoline *N*-oxide, and the synthetic antibiotics carbadox and olaquindox, was carried out with a hybrid quadrupole/time-of-flight (TOF) mass spectrometer coupled with electrospray (ES) and atmospheric pressure chemical ionization (APCI) sources. The full scan mass spectra of the *N*-oxides obtained with ES are similar to those obtained with APCI, and the characteristic fragment ions corresponding to $[M + H - O]^{+\bullet}$ were observed in the full scan mass spectrum of each *N*-oxide examined. The protonated molecule of each *N*-oxide was subjected to collision-induced dissociation (CID) and accurate mass measurements were made of each fragment ion so as to determine its elemental composition. Fragment ions generated at enhanced cone voltages upstream of the first mass-resolving element were subjected to CID so as to identify the direct product ion–precursor ion relationship. Plausible structures have been proposed for most of the fragment ions observed. Elimination of $OH^{\bullet}$ radicals generated from the N → O functional group is a characteristic fragmentation pathway of the *N*-oxides. The expulsion of radicals and small stable molecules is accompanied by formation and subsequent contraction of heterocyclic rings.

Keywords: Accurate mass; Tandem mass spectrometry; *N*-oxides; Time-of-flight; ES

1. Introduction

N-Oxides form an important family of compounds that are used as pharmaceuticals, agrochemicals, intermediates in synthetic chemistry, and as ligands in metal complexes [1,2]. *N*-Oxides are common metabolites because they can be formed by N atom oxidation of many drugs and xenobiotics [3,4]. Pharmaceutical products and their metabolites have become of general public concern due to their potential impacts to the environment [5,6], and *N*-oxides have generated particular interest due to their carcinogenic [3] and/or toxicological effects [7]. In the determination of trace levels of such environmental contaminants, unambiguous identification is critical; tandem mass spectrometry is an effective technique with both high sensitivity and high specificity for the measurement and identification of such compounds. In this study, three *N*-oxides, quinoline *N*-oxide, carbadox [3-(2-quinoxalinyl-methylene)carbazic acid methyl ester *N*, *N*′-dioxide], and olaquindox [*N*-(2-hydroxyethyl)-3-methyl-2-quinoxalinecarboxamide-1,4-dioxide] (Scheme 1) were chosen for study because they are illustrative of the mass spectrometric behavior of this class of compounds. Note that in Scheme 1, the heterocyclic ring bonds in quinoline *N*-oxide are numbered with a small font.

Quinoline *N*-oxide has been shown to be a microbiological oxidation product of quinoline [8], which is a principal azaarene found in smoke generated by the incomplete combustion of fuels [9] and in waters polluted by creosote [10]. Carbadox is an antibiotic approved in the 1970s for use in swine to prevent and treat disease as well as to maintain weight gain during periods of stress, such as weaning. Carbadox and one of its metabolites, desoxycarbadox, are suspected carcinogens and mutagens [11]. However, when

* Corresponding author. Tel.: +1-705-748-1011extn.5886; fax +1-705-748-1625.
E-mail addresses: xmiao@trentu.ca (X.-S. Miao), rmarch@trentu.ca (R.E. March), cmetcalfe@trentu.ca (C.D. Metcalfe).

1387-3806/$ – see front matter © 2003 Elsevier B.V. All rights reserved.
doi:10.1016/j.ijms.2003.08.012

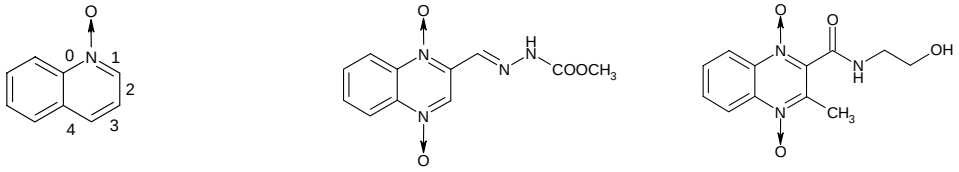

Quinoline N-oxide	Carbadox	Olaquindox
C_9H_7NO	$C_{11}H_{10}N_4O_4$	$C_{12}H_{13}N_3O_4$
145.0528[a]	262.0702	263.0906

[a] Monoisotope molecular weight

Scheme 1. Molecular structures of the *N*-oxides.

an appropriate withdrawal period (i.e., administration of the drug is arrested some time before slaughter) is observed, the drug and its breakdown products are not found in meat derived from the treated animal. Olaquindox is another synthetic antibiotic (effective against Gram-negative bacteria) and is used solely as a growth promoter [12]. For example, the consumption of olaquindox is 20 t per year in Denmark [13]. Olaquindox is photosensitive, so that reactive oxaziridine is formed by exposure to UV radiation [14]. Environmental impacts of residues of olaquindox have been examined recently [15–17].

Time-of-flight (TOF) analyzer systems have seen a revival during the last decade, mainly due to advances in high-speed electronics [18]. With the development of orthogonal acceleration reflectron-type TOF analyzers, resolving power exceeding 10,000 has become possible. TOF instruments have advantages over quadrupole mass spectrometers because the mass scale is established using the arrival time of individual ions, so that useful mass spectra with good mass accuracy can be obtained even when ion statistics are lower than on triple-quadrupole instruments [19,20]. In this work, a hybrid quadrupole/TOF mass spectrometer with electrospray (ES) and atmospheric pressure chemical ionization (APCI) sources was applied to a study of the tandem mass spectrometric behavior of the *N*-oxides, quinolone *N*-oxide, carbadox, and olaquindox. The interpretation of mass spectra is a key part of compound identification, and the combination of tandem mass spectrometry with high-resolution mass measurements can yield crucial information on the identity of a compound [21,22]. Therefore, accurate mass measurements were made of fragment ions so as to determine the elemental composition of fragment ions and to provide a basis for the proposal of fragmentation mechanisms of the protonated *N*-oxides.

2. Experimental

2.1. Materials

Quinoline *N*-oxide and carbadox were purchased from Sigma-Aldrich Canada (Oakville, Ont., Canada), and olaquindox was obtained from ICN Biomedicals Inc. (Aurora, OH, USA). Methanol and HPLC-grade water were purchased from Fisher Scientific Ltd. and EM Science Inc. (Gibbstown, NJ, USA), respectively. The analyte solutions were prepared using methanol and water (1:1) at a concentration of 100 $\mu g\,ml^{-1}$.

2.2. Mass spectrometry

Mass spectrometric analysis was performed using a Q-TOF II^{TM} mass spectrometer, which consists of a quadrupole mass filter and quadrupole collision cell coupled to a high-resolution reflectron TOF analyzer system, equipped with Z-spray^{TM} ES and APCI sources (Micromass, Manchester, UK). The capillary voltage in the ES source and the corona voltage in the APCI source were 3.0 and 4.0 kV, respectively. The sampling cone voltage was varied from 20 to 140 V for generation of mass spectra, and the specific value of the collision energy for each collision-induced dissociation (CID) experiment is given in the text or figures. The quadrupole mass filter to the TOF analyzer was set with LM and HM resolution of 15.0 (arbitrary units), which is equivalent to a 1.0 Da mass window for transmission of precursor ions. The source block and desolvation temperatures were set at 80 and 150 °C, respectively, for the ES source, and at 100 and 250 °C, respectively, for the APCI source. All single analyzer mass spectra were obtained by scanning the TOF analyzer. Fragmentations of the mass-selected ions were performed in an rf-only quadrupole collision cell with UHP argon as collision gas at 10 psi inlet pressure. Signal detection was performed with a reflector, microchannel plate (MCP) detector, and time-to-digital converter. Multi-point mass calibration was carried out using a mixture of NaI/RbI from *m*/*z* 50–1000 in positive-ion mode. Data acquisition and processing were carried out using the MassLynx NT version 3.5 software supplied with the instrument. The MS survey range was *m*/*z* 50–1000, with a scan duration of 1.0 s and an interscan delay of 0.1 s. Each mass spectrum was recorded in continuum mode over a period of 1 s and mass spectra were accumulated over a period of at least 60 s for both single analyzer profiles and CID experiments. Solutions of *N*-oxides were infused to

the ES or APCI sources using a Harvard Apparatus Model 11 syringe pump (Harvard Apparatus, Holliston, MA) at a flow rate of 10 μl min^{-1}.

As part of the software suite provided with the instrument, one can interrogate a product ion mass spectrum and generate an elemental composition report for each of the fragment ions. In the case where more than one formula is proposed, the formula shown is the one matching the proposed structure; the rationalization for selecting one structure over another is discussed below. A threshold of 5 mDa was set as a limit to the calculation of possible elemental compositions as it was expected that the accurate mass of a fragment ion would lie within a window of ±5 mDa of the exact mass. A mass measurement of 5 ppm for an ion of *m/z* 100 corresponds to a mass error of 0.5 mDa, but the timing of ions of such low mass/charge ratio is somewhat problematic and the situation is confounded when the ion signal intensity for such ions is low. The correct functioning of the centroiding process that is required for mass measurement relies upon a symmetric peak shape that is not observed invariably for ions of such low ion signal intensity. The inherent stability of the TOF analyzer allows mass accuracy of better than 50 ppm using just an external 2-point calibration, but mass accuracy may be improved further by including an internal calibration point or lock mass [23]. In this study, because the parent molecule is a known entity, the precursor ion was used as a lock mass in the product ion mass spectrum.

3. Results and discussion

Mass spectra were obtained with each of the ES and APCI ion sources. Because the signal intensities of negative ions of *N*-oxides were so low (data not shown), only the study conducted in positive-ion mode is reported. Fig. 1a and b shows respectively the full scan mass spectra of olaquindox obtained with each of ES and APCI sources. The two mass spectra differ with respect to the degree of fragmentation, which is greater for APCI, the relative intensities of fragment ions, and the presence of sodiated ion $[M + Na]^+$ which is observed with ES only. Similar observations were made from the ES and APCI mass spectra of quinoline *N*-oxide and carbadox.

The ion corresponding to the loss of an oxygen atom from the protonated molecule, $[M + H - O]^{\bullet +}$, was observed in each of the full scan mass spectra of the three analytes with ES and APCI (Fig. 1); that is, ions at *m/z* 130, 247, and 248 corresponding to $[M + H - O]^{\bullet +}$ were observed in the full scan spectra of quinoline *N*-oxide, carbadox, and olaquindox, respectively. The formation of $[M + H - O]^{\bullet +}$ ions from the protonated *N*-oxides is most likely due to the thermal degradation of the N → O functional group of the *N*-oxides.

An intense ion signal corresponding to the sodiated ion $[M + Na]^+$ was observed at *m/z* 168 in the full scan mass spectrum of quinoline *N*-oxide. An attempt to produce a product ion mass spectrum from $[M + Na]^+$ was not successful as no fragment ions were observed upon CID. The inability to fragment the $[M + Na]^+$ ion is probably due to the strong affinity between the sodium ion and quinoline *N*-oxide resulting from the large dipole moment of quinoline *N*-oxide. It has been observed in this laboratory on several occasions that sodiated molecules are more resistant to fragmentation than are protonated molecules. Although the sodiated molecules of carbadox and olaquindox could be dissociated, little valuable structural information could be obtained from these product ion mass spectra. In the following discussion, only product ion mass spectra of the three protonated *N*-oxide molecules are examined.

3.1. Quinoline N-oxide

Due to the similarity of full scan mass spectra and product ion mass spectra of the analytes obtained with each of ES and APCI, the following discussion is independent of source. Fig. 2 shows the product ion mass spectrum of protonated quinoline *N*-oxide; the fragmentation pathways proposed to account for the ions observed in Fig. 2 are shown in Scheme 2. To assign the elemental composition of fragment ions, the ES-MS/MS spectrum of protonated quinoline *N*-oxide was acquired using exact mass measurements, and the precursor ion $[M+H]^+$ was selected as a lock mass (*m/z*

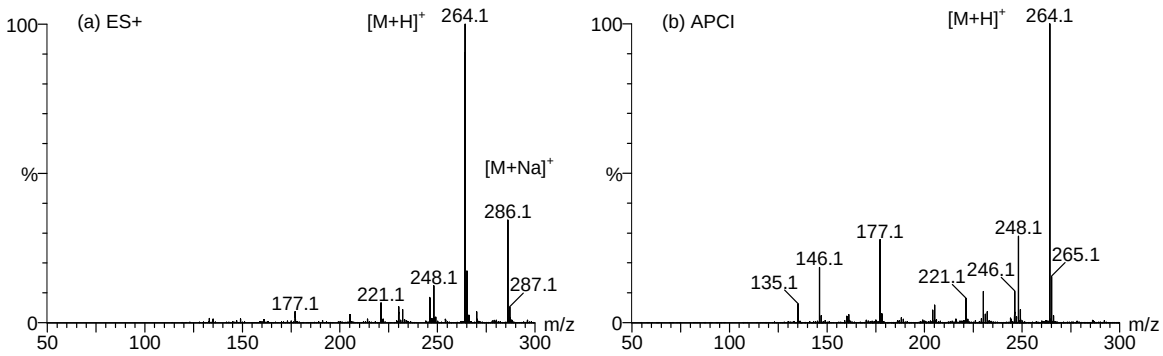

Fig. 1. Mass spectra of olaquindox in positive-ion mode with ES and APCI. (a) ES: capillary 3.0 kV, cone 30 V, (b) APCI: corona 4.0 kV, cone 30 V.

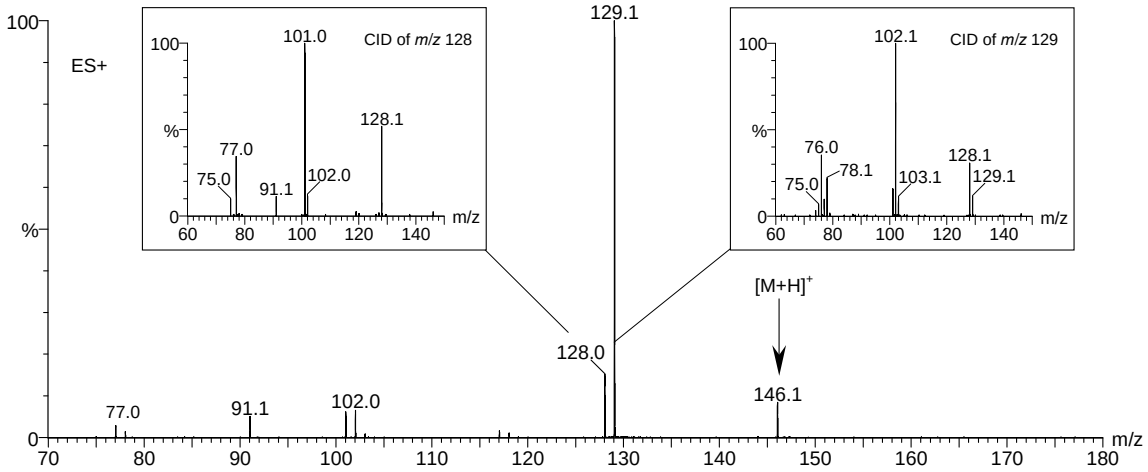

Fig. 2. Product ion mass spectrum of protonated quinoline *N*-oxide. Cone voltage 50 V, collision energy 25 eV. The peak labeled with a vertical arrow is the precursor ion. The inset (left side) is the product ion mass spectrum of ion *m*/*z* 128, which was conducted at cone 60 V and collision energy 20 eV. The inset (right side) is the product ion mass spectrum of ion *m*/*z* 129, which was conducted at cone 60 V and collision energy 30 eV.

146.0528). Table 1 lists the formula, observed mass, calculated mass, and mass error for the fragment ions observed in the MS/MS spectra of the protonated quinoline *N*-oxide. The errors between the observed masses and calculated ones ranged from −0.5 to 0.1 mDa (−4.9 to 1.0 ppm), with an average value of 0.2 mDa (2.4 ppm), indicating good mass accuracy.

The base peak in the product ion mass spectrum is the ion species of *m*/*z* 129, corresponding to the elimination of an OH• radical. The protonated quinoline *N*-oxide molecule with an electron-attracting N → O group can be stabilized by elimination of the oxygen atom as an OH• radical, as was observed previously [24]. The "deoxygenation" process is associated with thermal activation and does not result from

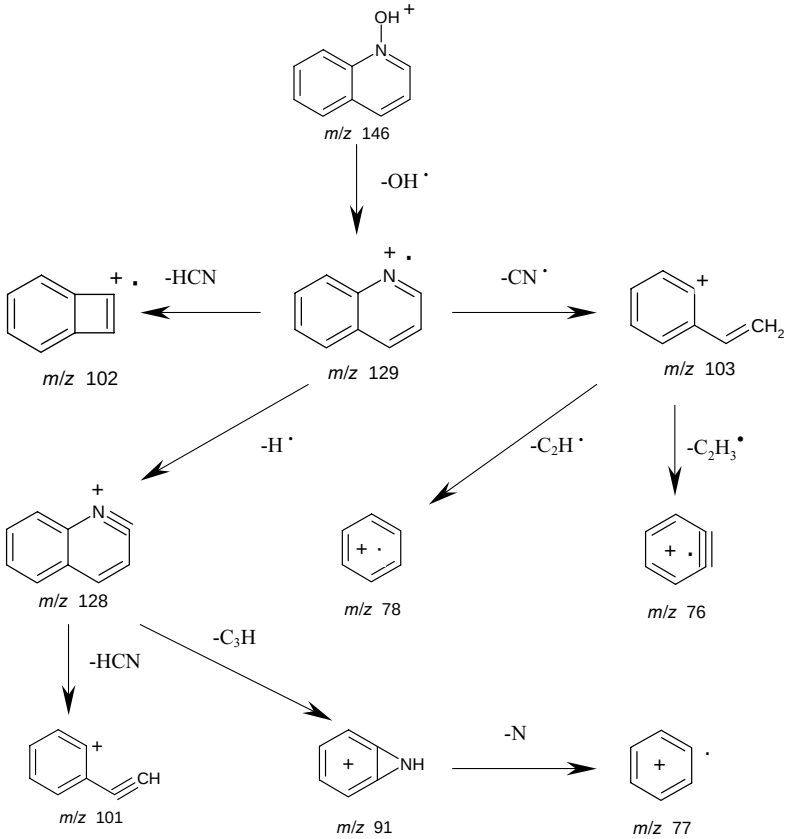

Scheme 2. Proposed fragmentation pathways of quinoline *N*-oxide.

Table 1
Formula, observed and calculated mass, double bond equivalents (DBE), and mass error of the fragment ions in the MS/MS spectrum of protonated quinoline *N*-oxide

Predicted formula	Observed mass (Da)	Calculated mass (Da)	DBE	Error (mDa)	Error (ppm)
$C_9H_8NO^+$	146.0606	146.0606	6.5	–	–
$C_9H_7N^+$	129.0578	129.0578	7.0	0.0	0.0
$C_9H_6N^+$	128.0500	128.0500	7.5	0.0	0.0
$C_8H_7^+$	103.0543	103.0548	5.5	−0.5	−4.8
$C_8H_6^+$	102.0471	102.0470	6.0	+0.1	+1.0
$C_8H_5^+$	101.0386	101.0391	6.5	−0.5	−4.9
$C_6H_6^+$	78.0468	78.0470	4.0	−0.2	−2.6
$C_6H_5^+$	77.0388	77.0391	4.5	−0.3	−3.9
Average				0.2	2.4

collisional activation in the desolvation region of the API source. Thus, the ion corresponding to $[M+H-O]^{\bullet+}$ (*m*/*z* 130 for quinoline *N*-oxide) in the full scan mass spectrum was not observed in the product ion mass spectrum.

The loss of a H atom has been observed frequently while using an EI source [25,26]; however, there are few reports of the observation of H atom loss with an ES source [27]. The inset of Fig. 2 shows the product ion mass spectrum of ion *m*/*z* 129, which clearly indicates that ion *m*/*z* 128 is produced by expulsion of a hydrogen atom from *m*/*z* 129. The precursor ion *m*/*z* 129 was selected at unit resolution with the quadrupole analyzer, so as to exclude the transmission of *m*/*z* 128 from contaminant ions. The ion species of *m*/*z* 102 and 103 were generated by the loss of the imino group from ion *m*/*z* 129 as hydrogen cyanide (HCN, 27 Da) with the subsequent ring contraction, and the loss of $CN^{\bullet}$ radical, respectively. The observation of *m*/*z* 76 and 78 is thought to occur by losses of $C_2H_3^{\bullet}$ (27 Da) and $C_2H^{\bullet}$ (25 Da), respectively, from *m*/*z* 103.

The ion species of *m*/*z* 128 generated ions at *m*/*z* 101 by loss of HCN (27 Da). The ion signals due to *m*/*z* 91 were very weak and accurate mass measurement was not possible. This ion species cannot be identified as $C_7H_7^+$ because its precursor ion, *m*/*z* 128, has but six hydrogen atoms. The proposed structure for *m*/*z* 91 shown in Scheme 2 involves the loss of a $C_3H^{\bullet}$ moiety. Ion of *m*/*z* 77 is formed by the expulsion of nitrogen atom from *m*/*z* 91.

The initial loss of an $OH^{\bullet}$ radical (and, possibly, C_2HNO) from protonated quinoline *N*-oxide is followed by competing fragmentations that involve radicals and HCN molecules.

3.2. Carbadox

The weakness of the N → O bond indicates a high propensity for the elimination of the $OH^{\bullet}$ radical species from protonated carbadox. Fig. 3 shows the product ion mass spectrum of protonated carbadox; the fragmentation pathways of protonated carbadox are proposed in Scheme 3. In Scheme 3, the fragmentation pathways are characterized by the expulsion of radicals, such as $O^{\bullet\bullet}$, $OH^{\bullet}$ and $CN^{\bullet}$ species. Table 2 lists the formula, observed and calculated masses, and mass errors of the fragment ions in the ES-MS/MS spectrum of protonated carbadox that were observed by using the precursor ion $[M+H]^+$ (263.0780) as a lock mass. The errors between the observed masses and calculated ones ranged from −4.7 to 3.5 mDa (−25 to 20 ppm)

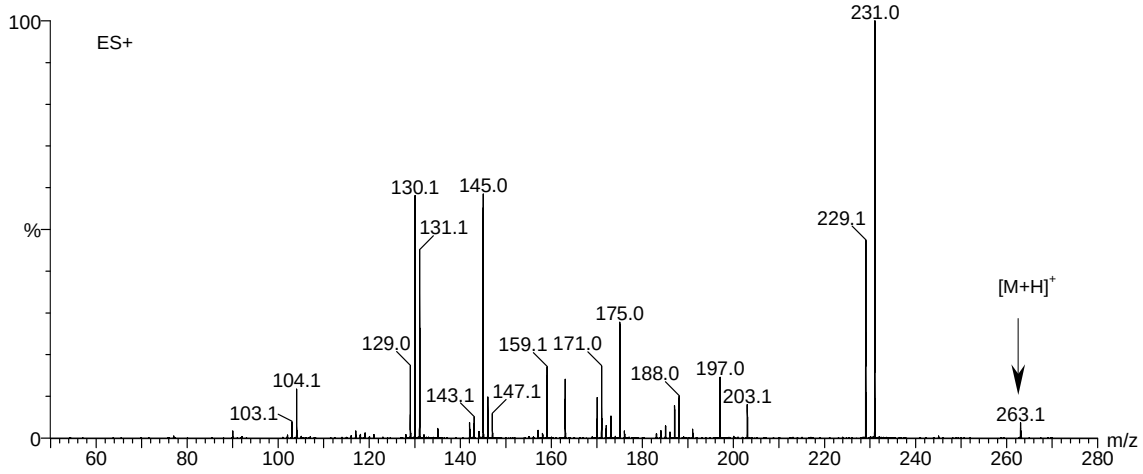

Fig. 3. Product ion mass spectrum of $[M+H]^+$ from carbadox. Cone 30 V, collision energy 22 eV. The peak labeled with a vertical arrow is the selected precursor ion.

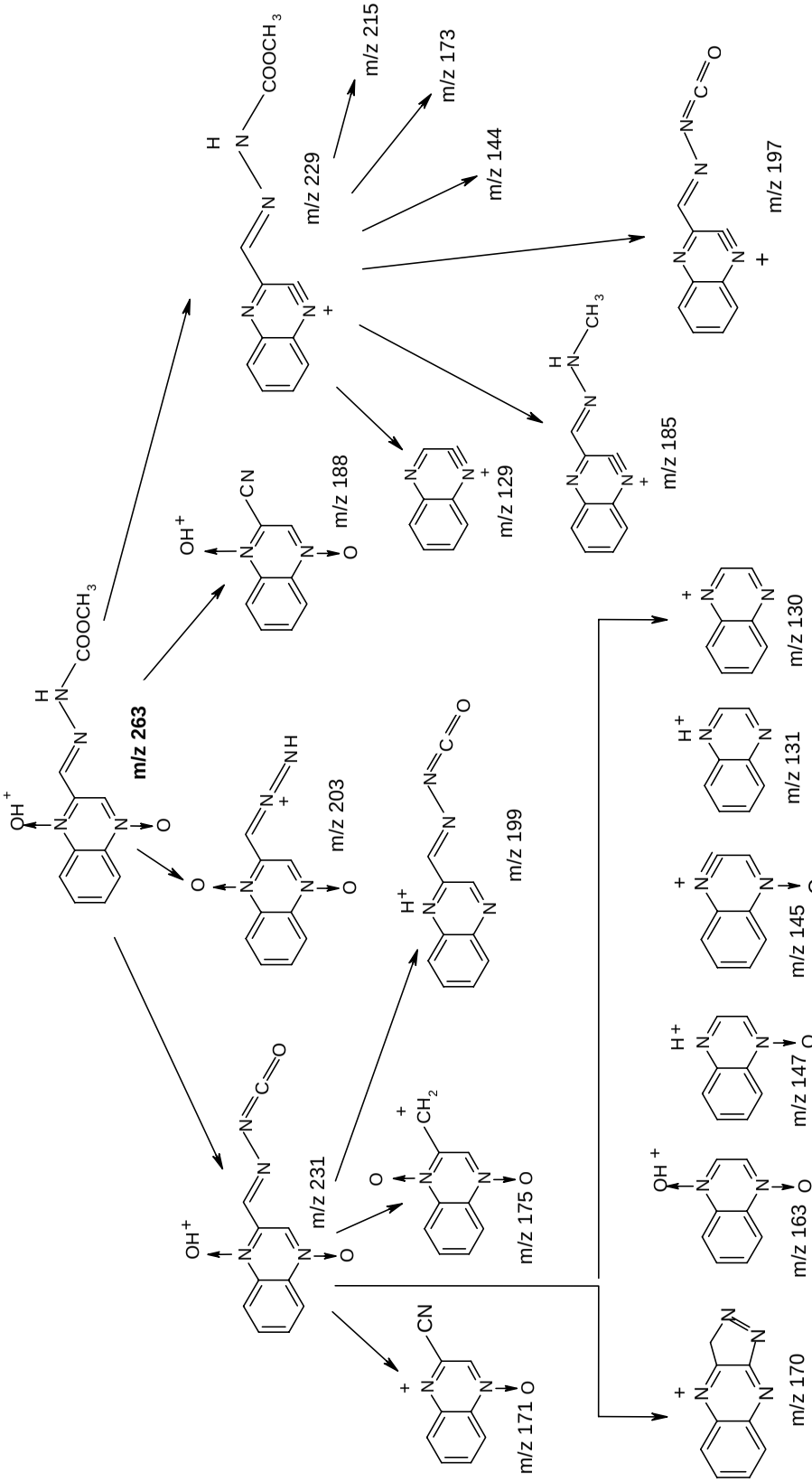

Scheme 3. Proposed fragmentation pathways of carbadox.

Table 2
Formula, observed and calculated mass, double bond equivalents (DBE), and mass error of the fragment ions in the MS/MS spectrum of protonated carbadox

Predicted formula	Observed mass (Da)	Calculated mass (Da)	DBE	Error (mDa)	Error (ppm)
$C_{11}H_{11}N_4O_4^+$	263.0780	263.0780	8.5	–	–
$C_{10}H_7N_4O_3^+$	231.0518	231.0518	9.5	0.0	0.0
$C_{11}H_9N_4O_2^+$	229.0720	229.0726	9.5	−0.6	−2.6
$C_{10}H_7N_4O_2^+$	215.0560	215.0569	9.5	+0.9	+4.2
$C_9H_7N_4O_2^+$	203.0566	203.0569	8.5	−0.3	−1.5
$C_{10}H_7N_4O^+$	199.0637	199.0620	9.5	+1.7	+8.5
$C_{10}H_5N_4O^+$	197.0466	197.0463	10.5	+0.3	+1.5
$C_9H_6N_3O_2^+$	188.0460	188.0460	8.5	0.0	0.0
$C_{10}H_9N_4^+$	185.0780	185.0827	8.5	−4.7	−25.0
$C_9H_7N_2O_2^+$	175.0511	175.0508	7.5	+0.4	+2.3
$C_{10}H_9N_2O^+$	173.0750	173.0715	7.5	+3.5	+20.0
$C_9H_5N_3O^+$	171.0430	171.0433	9.0	−0.3	−1.8
$C_9H_6N_4^+$	170.0610	170.0592	9.0	+1.8	+11.0
$C_8H_7N_2O_2^+$	163.0510	163.0508	6.5	+0.2	+1.2
$C_8H_7N_2O^+$	147.0565	147.0558	6.5	+0.7	+4.8
$C_8H_5N_2O^+$	145.0399	145.0402	7.5	−0.3	−2.1
$C_9H_8N_2^+$	144.0720	144.0687	7.0	+3.3	+23.0
$C_8H_7N_2^+$	131.0614	131.0609	6.5	+0.4	+3.1
$C_8H_6N_2^+$	130.0544	130.0531	7.0	+1.3	+10.0
$C_8H_5N_2^+$	129.0473	129.0453	7.5	+2.0	+16.0
Average				1.2	7.3

with an average value of 1.2 mDa (7.3 ppm); such small errors permit the identification of a consistent group of fragment ions which form the basis for the proposed fragmentation pathways shown in Scheme 3. It should be noted that a mass defect of 1.0 mDa for an ion of low mass/charge ratio, say *m*/*z* 200, yields an error of 5 ppm which is not inordinately high for small mass/charge ratio ions. Furthermore, for an ion of *m*/*z* 200, there are few different elemental compositions that satisfy the elemental requirements of the known parent ion, and therefore the elemental composition of a fragment ion can be obtained with a high degree of confidence.

Carbadox is a dioxide and so the loss of two $OH^\bullet$ radicals from protonated carbadox (*m*/*z* 263) is expected and, indeed, the loss of two $OH^\bullet$ radicals to yield *m*/*z* 229 is observed. However, the loss of a single $OH^\bullet$ was not observed; only the concerted loss of H_2O_2 was observed. Furthermore, the loss of CH_3OH from the side chain to form the base peak at *m*/*z* 231 exceeded the loss of $OH^\bullet$ radicals. The base peak observed at *m*/*z* 231 could be produced either by the loss of CH_3OH (32 Da) or two oxygen atoms (32 Da); the correct choice can be elucidated readily from the accurate masses listed in Table 2. Here, the accurate mass of formula $C_{10}H_7N_4O_3^+$ corresponding to the loss of CH_3OH is 231.0518 Da, whereas the accurate mass of $C_{11}H_{11}N_4O_2^+$ corresponding to the loss of two oxygen atoms is 231.0882 Da. The error between the observed and calculated masses for the former fragment ion is 0.0 mDa whereas the corresponding error for the latter fragment ion is 36.0 mDa, thus the correct choice is loss of CH_3OH. In addition, the hydroxyl group on the side chain probably is the site of lowest proton affinity of the molecule and the elimination of CH_3OH is favored, as expected. Losses of $HCOOCH_3$ and $H_2NCOOCH_3$ from the side chain yielded fragment ions of *m*/*z* 203 and *m*/*z* 188, respectively. Only minor fragmentation corresponding to elimination of H_2O from $[M + H]^+$ was observed.

Fragment ions were investigated in order of descending mass/charge ratio so as to determine the direct product ion–precursor ion relationship for each product ion. Only four fragment ion species, *m*/*z* 231, 229, 203, and 188, are formed directly from protonated carbadox upon CID. Each of these species was selected by the first mass-resolving element (quadrupole mass filter) and subjected to further CID once the ion signal intensity of the ion species of interest had been optimized by adjustment of the cone voltage. The utilization of enhanced cone voltage to optimize first generation fragment ion signal intensity can yield pseudo-MS/MS/MS performance in the Q-TOF II™ mass spectrometer that is useful in determining the hierarchy of fragment ions. In the examination of a standard substance, such as carbadox, the probably of isolating isobaric fragment ions in the first quadrupole mass filter is zero when such ions are not detected in the initial product ion mass spectrum.

CID of *m*/*z* 188 and *m*/*z* 203 yielded fragment ions of such low signal intensity that elemental composition could not be determined with precision. CID of *m*/*z* 231 yielded nine fragment ions of sufficient ion signal intensity to permit both determination of the precise mass/charge ratio and calculation of elemental composition, as shown in Table 2. The fragment ion structures shown in Scheme 3 are plausible but are not definitive. In the creation of ion structures, one is constrained normally by the structure of the precursor ion, normal valencies of constituent atoms and, for the *N*-oxide

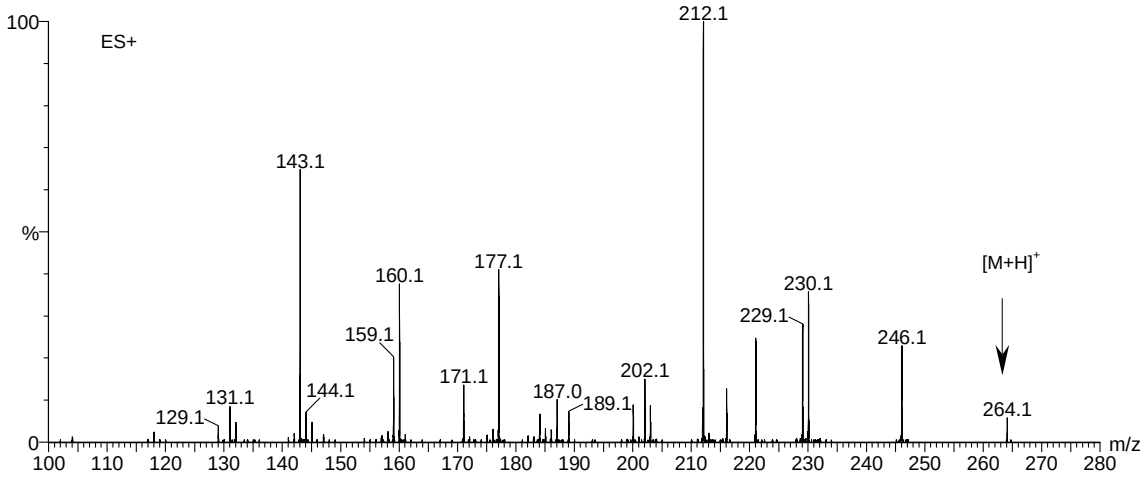

Fig. 4. Product ion mass spectrum of protonated olaquindox $[M+H]^+$. Cone 30 V, collision energy 23 eV. The peak labeled with a vertical arrow is the selected precursor.

fragment ions, the high degree of unsaturation. Within these constraints, particularly the high degree of unsaturation, the choice of structure is often one in which severe strain can be expected. Preliminary molecular orbital calculations indicate that some strained species can, nevertheless, exist in minima on the potential-energy surface. The neutral losses in each case can be determined from Table 2. Only three ion species, *m*/*z* 171, 175, and 199, must necessarily be direct fragments of *m*/*z* 231; the remaining six species are not necessarily direct fragments of *m*/*z* 231 and are shown in Scheme 3 below the three species formed directly from *m*/*z* 231. CID of *m*/*z* 229 yielded six fragment ions also of sufficient ion signal intensity to permit both determination of the precise mass/charge ratio and calculation of elemental composition, as shown in Table 2. Only *m*/*z* 197 and *m*/*z* 185 must necessarily be direct fragments of *m*/*z* 229. None

Table 3
Formula, observed mass and calculated mass, double bond equivalents (DBE), and mass error of the fragment ions in the MS/MS spectrum of protonated olaquindox

Predicted formula	Observed mass (Da)	Calculated mass (Da)	DBE	Error (mDa)	Error (ppm)
$C_{12}H_{14}N_3O_4^+$	264.0984	264.0984	7.5	–	–
$C_{12}H_{12}N_3O_3^+$	246.0878	246.0879	8.5	−0.1	−0.4
$C_{12}H_{12}N_3O_2^+$	230.0929	230.0930	8.5	−0.1	−0.4
$C_{12}H_{11}N_3O_2^+$	229.0852	229.0851	9.0	+0.1	+0.4
$C_{10}H_9N_2O_4^+$	221.0561	221.0562	7.5	−0.1	−0.5
$C_{12}H_{11}N_3O^+$	213.0914	213.0902	9.0	+1.2	+5.6
$C_{12}H_{10}N_3O^+$	212.0828	212.0824	9.5	+0.4	+1.9
$C_{10}H_8N_3O_2^+$	202.0626	202.0617	8.5	+0.9	+4.5
$C_{11}H_8N_3O^+$	198.0718	198.0667	9.5	+5.1	+26.0
$C_{10}H_7N_2O_2^+$	187.0535	187.0508	8.5	+2.7	+14.0
$C_{10}H_8N_3O^+$	186.0643	186.0667	8.5	−2.4	−13.0
$C_{10}H_7N_3O^+$	185.0638	185.0589	9.0	+4.8	+26.0
$C_{11}H_{10}N_3^+$	184.0856	184.0875	8.5	−1.9	−10.0
$C_9H_9N_2O_2^+$	177.0672	177.0664	6.5	+0.8	+4.5
$C_{10}H_7N_2O^+$	171.0564	171.0558	8.5	+0.5	+2.9
$C_{10}H_8N_3^+$	170.0758	170.0718	8.5	+4.0	+24.0
$C_9H_8N_2O^+$	160.0658	160.0637	7.0	+2.1	+13.0
$C_9H_7N_2O^+$	159.0588	159.0558	7.5	+3.0	+19.0
$C_{10}H_9N_2^+$	157.0769	157.0766	7.5	+0.3	+1.9
$C_{10}H_8N_2^+$	156.0693	156.0687	8.0	+0.6	+3.8
$C_8H_5N_2O^+$	145.0431	145.0402	7.5	−2.9	−20.0
$C_9H_8N_2^+$	144.0688	144.0687	7.0	+0.1	+0.7
$C_9H_7N_2^+$	143.0636	143.0609	7.5	+2.7	+19.0
$C_8H_6NO^+$	132.0459	132.0449	6.5	+1.0	+7.6
$C_8H_7N_2^+$	131.0626	131.0609	6.5	+1.7	+13.0
$C_7H_6N_2^+$	118.0545	118.0531	6.0	+1.4	+12.0
Average				1.6	9.8

of the fragments observed was formed by scission of the heterocyclic ring.

3.3. Olaquindox

Fig. 4 shows the product ion mass spectrum of protonated olaquindox; its fragmentation pathways are proposed in Scheme 4. Table 3 lists the formula, observed and calculated masses, and mass errors of the fragment ions in the ES-MS/MS spectrum of protonated olaquindox that were observed by using the precursor ion $[M + H]^+$ (264.0984) as a lock mass. The errors between the calculated and observed masses range from −2.9 to 5.1 mDa (−20 to 26 ppm) with an average value of 1.6 mDa (9.8 ppm).

It was anticipated that the terminal hydroxy group on the side chain of olaquindox would permit the observation of water loss and that the methyl group on the heterocyclic ring would inhibit loss of an $OH^\bullet$ from its adjacent N → O group. As shown in Fig. 4, protonated olaquindox loses H_2O to form *m/z* 246 and loses two $OH^\bullet$ radicals in a concerted action as H_2O_2 to form *m/z* 230. The combined effect of these competing reactions is the formation of *m/z* 212 (by loss of H_2O_2 and H_2O in order only) as the base peak. Thus, the concerted loss of $2OH^\bullet$ was not impeded by the introduction of the methyl group; possibly, a hydrogen atom was transferred to the N → O from the methyl group.

Only three fragment ion species, *m/z* 246, 230, and 221, are formed directly from protonated olaquindox upon CID. Each of these species was selected in the quadrupole mass filter and subjected to further CID once the ion signal intensity of the ion species of interest had been optimized by adjustment of the cone voltage as for the investigation

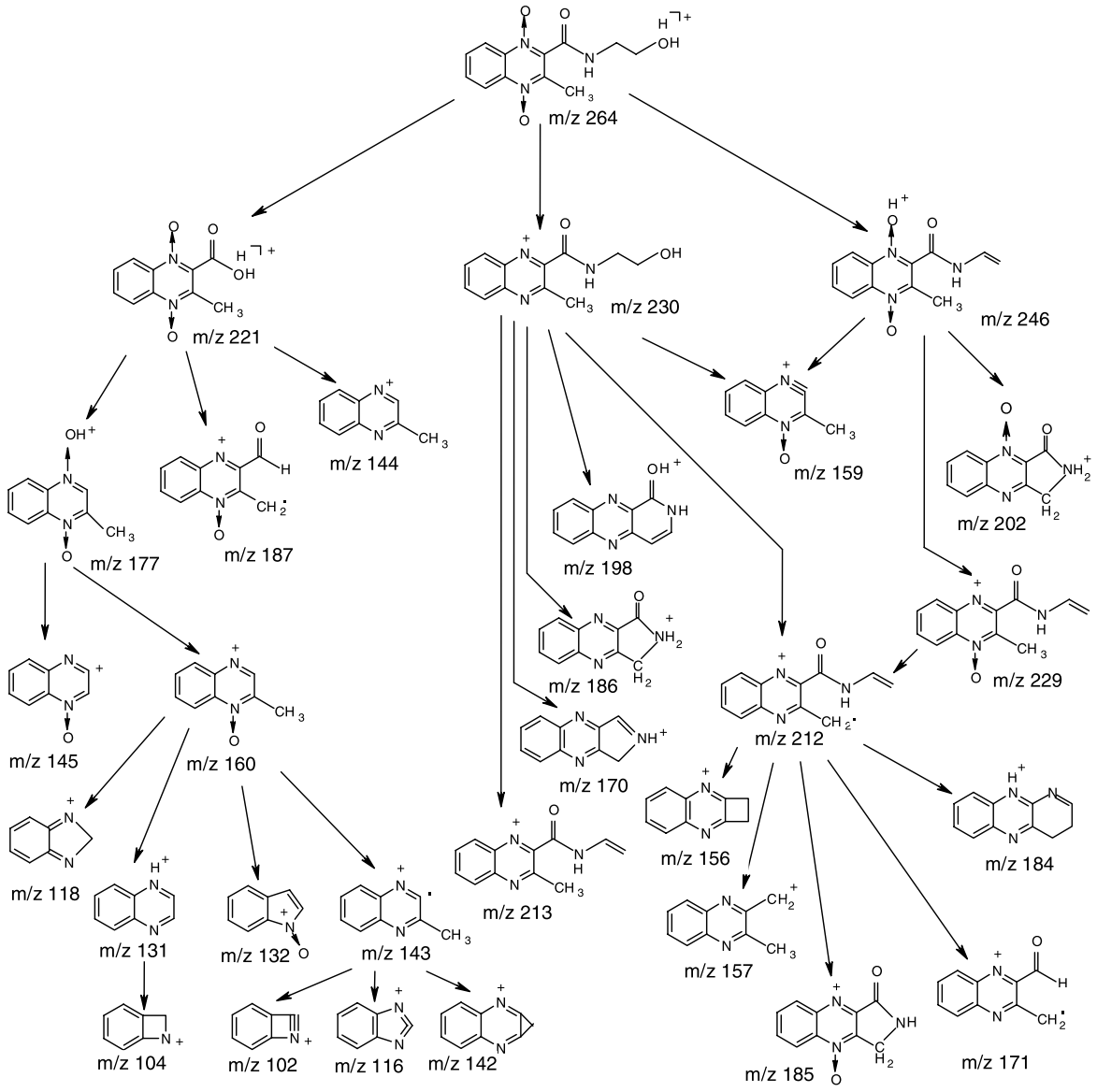

Scheme 4. Proposed fragmentation pathways of olaquindox.

of carbadox. This process of isolation of fragment ions in the first quadrupole mass filter and subsequent CID was repeated until the ion signal intensity was insufficient to yield useful information on the next generation of fragment ions. For each of the arrows shown in Scheme 4, the direct product ion–precursor ion relationship was observed. Because the ion signal intensities of some fragment ions were conveniently high, it was possible to determine five generations of fragment ions in the most favorable case; that of *m*/*z* 264 → *m*/*z* 221 → *m*/*z* 177 → *m*/*z* 160 → *m*/*z* 143 → *m*/*z* 102, 116, and 142.

The fragment ion structures shown in Scheme 4 are plausible but are not definitive. The neutral losses corresponding to each product ion–precursor ion relationship identified can be determined from Table 3; these losses are primarily small stable molecules, such as H_2O, HCN, CH_3OH, CO, CO_2, and C_2H_2O together with radicals, such as $OH^{\bullet}$, $CHO^{\bullet}$ and $C_2H_3^{\bullet}$. The most unusual loss is that of $CHO_4^{\bullet}$ from *m*/*z* 221 to form *m*/*z* 144. It is of interest to note that the dioxide moiety can survive two fragmentations and occurs in *m*/*z* 177, while an oxide moiety can survive four fragmentations and occurs in *m*/*z* 132. The formation of *m*/*z* 177 corresponds to the loss of the complete side chain. Due to radical expulsion from the side chain, the side chain tends to form five- and 6-membered rings which is energetically favored due to π-bond formation within the three systems and the electrophilic effect of NH in the side chain.

Scission of the heterocyclic ring in the respective precursor ions could account for the formation of several fragment ions. Ions of *m*/*z* 116 and 118 may be formed by 2,3 scission, *m*/*z* 132 by 0,1 scission, and *m*/*z* 102 and 104 by 0,3 scission. No $[M+H-O]^+$ ions were observed in the product ion mass spectra of the protonated compounds, although they were observed in the full scan mass spectra of the compounds.

3.4. Comparison of fragmentations

In protonated quinoline *N*-oxide, the N → O functional group is destroyed by the loss of a hydroxyl radical in the primary fragmentation. Subsequent fragmentation occurs in the nitrogen-containing ring until hydrogenated rings of six carbon atoms remain. For protonated carbadox and olaquindox, the base peak in each product ion mass spectrum (Figs. 3 and 4, respectively) is formed by fragmentation of the side chain and the *N*-oxide functionality has remained intact. Indeed, the N → O functional group can remain intact throughout several fragmentation stages. This observation may indicate retention of the N → O functional group in metabolites of *N*-oxides with retention of biological activity not limited necessarily to the same level of activity as that of the parent compound. The consequence of retention of the N → O functional group throughout several fragmentation stages is the preferential step-wise loss of the side chains in carbadox and olaquindox. It remains to be determined whether side chains are as vulnerable to primary fragmentation when there is but a single N → O functional group in the ion.

4. Conclusions

In conclusion, we have presented complete fragmentation pathways for three protonated *N*-oxides using a hybrid quadrupole/TOF mass spectrometer with ES and APCI. The elemental composition of each fragment ion has been obtained by accurate mass analysis and plausible structures have been proposed for many of the fragment ions observed. It has been possible to product ion–precursor ion relationships for up to five generations of fragment ions by using an elevated cone voltage to generate fragments ions upstream of the first mass-selective element. An interesting feature of *N*-oxides is their ability to eliminate oxygen in the N → O functional group as $OH^{\bullet}$ radical species from $[M+H]^+$ ions; however, this elimination is not invariably a primary fragmentation process.

Acknowledgements

The authors acknowledge the financial support from each of the Natural Sciences and Engineering Research Council of Canada (Discovery Grants Program and Strategic Grants Program), the Canada Foundation for Innovation and the Ontario Innovation Trust.

References

[1] A.R. Katritzky, J.M. Lagowski, Chemistry of Heterocyclic *N*-oxides, Academic Press, London, 1971.
[2] A. Albini, S. Pietra, Heterocyclic *N*-Oxides. CRC, Boca Raton, 1991.
[3] T.R. Bosin, R.P. Maickel, Res. Commun. Chem. Pathol. Pharmacol. 6 (1973) 813.
[4] G.G. Gibson, P. Skett, Introduction to Drug Metabolism, Chapman and Hall, London, 1986.
[5] C.D. Metcalfe, X.-S. Miao, B.G. Koenig, J. Struger, Environ. Chem. Toxicol. (2003) (in press).
[6] X.-S. Miao, C.D. Metcalfe, Anal. Chem. 75 (2003) 3731.
[7] M. Kiese, Pharmcol. Rev. 18 (1966) 1091.
[8] J.B. Sutherland, J.P. Freeman, A.J. Williams, C.E. Cerniglia, Exp. Mycol. 18 (1994) 271.
[9] M.W. Dong, D.C. Locke, D. Hoffmann, Environ. Sci. Technol. 11 (1977) 612.
[10] C.A. Krone, D.G. Burrows, D.W. Brown, P.A. Robisch, A.J. Friedman, D.C. Malins, Environ. Sci. Technol. 20 (1986) 1144.
[11] M.J. Hutchinson, P.Y. Young, S.A. Hewitt, D. Faulkner, D.G. Kennedy, Analyst 127 (2002) 342.
[12] M. Rabølle, N.H. Spliid, Chemosphere 40 (2000) 715.
[13] S.E. Jørgensen, H.C. Lützhøft, B.H. Sørensen, Ecol. Model. 107 (1998) 63.
[14] H. De Vries, J. Bajarski, A.A. Donker, A. Bakri, Toxicology 63 (1990) 85.
[15] C.A. Kan, M. Petz, J. Agric. Food Chem. 48 (2000) 6397.
[16] J. Tolls, Environ. Sci. Technol. 35 (2001) 3397.

[17] B. Halling-Sørensen, G. Sengeløv, F. Ingerslev, L.B. Jensen, Arch. Environ. Contam. Toxicol. 44 (2003) 7.
[18] C. Brunnée, Int. J. Mass Spectrom. Ion Processes 76 (1987) 125.
[19] J. Hau, M. Roberts, Anal. Chem. 71 (1999) 3977.
[20] C. Eckers, J.C. Wolf, N.J. Haskins, A.B. Sage, K. Giles, R. Bateman, Anal. Chem. 72 (2000) 3683.
[21] J. Hau, R. Stadler, T.A. Jenny, L.B. Fay, Rapid Commun. Mass Spectrom. 15 (2001) 1840.
[22] X.-S. Miao, R.E. March, C.D. Metcalfe, Rapid Commun. Mass Spectrom. 17 (2003) 149.
[23] A.P. Watt, A. Pike, D. Morrison, J. Am. Soc. Mass Spectrom. 12 (2001) 1145.
[24] W. Tong, S. Chowdhury, J.-C. Chen, R. Zhong, K.B. Alton, J.E. Patrick, Rapid Commun. Mass Spectrom. 15 (2001) 2085.
[25] S.M. Schildcrout, J.A. Reeder, Rapid Commun. Mass Spectrom. 11 (1997) 1457.
[26] W. Danikiewicz, K. Wojciechowski, Rapid Commun. Mass Spectrom. 10 (1996) 36.
[27] J.M.J. Nuutinen, M. Purmonen, J. Ratilainen, K. Rissanen, P. Vainiotalo, Rapid Commun. Mass Spectrom. 15 (2001) 1374.